MBE growth of Ge1-xSnx devices with intrinsic disorder

MBE growth of $Ge_{1-x}Sn_x$ devices with intrinsic disorder

S. N. Holmes[1(a)], Y. Gul[2], I. Pullen[2], J. Gough[2], K. J. Thomas[1(b)], H. Jia[1], M. Tang[1], H. Liu[1], M. Pepper[1,2]

[1] Department of Electronic and Electrical Engineering, University College London, Torrington Place, London, WC1E 7JE, United Kingdom.
[2] London Centre for Nanotechnology, University College London, 17-19 Gordon Street, London, WC1H 0AH, United Kingdom.

Abstract

We discuss the electrical properties of MBE (molecular beam epitaxy) grown, modulation doped, $Ge_{1-x}Sn_x$ quantum well devices. A consequence of the epitaxial growth process is that electronic disorder is introduced even in modulation doped quantum well structures and electrical transport properties that are characteristic of a high level of disorder are apparent. MBE growth of this material also results in the surface segregation of elemental β-Sn in the way that has been observed utilizing other epitaxial growth methods. A thermally activated, p-type mobility is a clear feature of the electrical properties with generally temperature independent hole densities $\sim 10^{12}$ cm^{-2} from the measured Hall effect and coming from the modulation doping. We present a discussion of Hall effect measurements in this disordered regime. The percolation carrier density in MBE modulation doped GeSn is in the region of $\sim 1\times10^{12}$ cm^{-2} although Hall measurements in this regime are difficult to quantify when the resistivity $> (h/e^2)$. In this notation h is Planck's constant and e is the unit of charge. Conductivities (σ) as low as $\sim 0.028\times(e^2/h)\times$square can be measured in the four-contact ac configuration and the temperature dependence indicates a mobility edge in these p-type devices below $\sim 2\times10^{12}$ cm^{-2}. At lower temperatures ($< \sim 1$ K) the presence of a Coulomb gap can be determined using dc transport, constant voltage measurements where small ac current excitation is not available experimentally. This two-contact configuration can determine σ down to $\sim 10^{-6}\times(e^2/h)$, deep into the localization regime, revealing a hopping conductivity dominated system. We discuss the relevance of these electrical properties for MBE grown GeSn devices.

(a) corresponding author email: stuart.holmes@ucl.ac.uk
(b) on leave from the Department of Physics, Central University of Kerala, Periye P. O., Kasargod District, PIN 671320, Kerala, India

Email addresses:
S. N. Holmes: stuart.holmes@ucl.ac.uk
Y. Gul: y.gul@ucl.ac.uk
I. Pullen: iwan.pullen.20@ucl.ac.uk
J. Gough: jonathan.gough.18@ucl.ac.uk
K. Thomas: kj_thomas@cukerala.ac.in
H. Jia: hui.jia@ucl.ac.uk
M. Tang: mingchu.tang@ucl.ac.uk
H. Liu: huiyun.liu@ucl.ac.uk
M. Pepper: michael.pepper@ucl.ac.uk

ORCID ids:
S. N. Holmes https://orcid.org/0000-0002-3221-5124
Y. Gul: https://orcid.org/0000-0003-2851-1374
K. Thomas: https://orcid.org/0000-0002-6901-2072
M. Tang: https://orcid.org/0000-0001-6626-3389
H. Liu: https://orcid.org/0000-0002-7654-8553
M. Pepper https://orcid.org/0000-0003-3052-5425

1. Introduction

1.1. Introduction to germanium-tin

Electrical transport properties of GeSn modulation doped devices fabricated by molecular beam epitaxy (MBE) are presented in this paper. We discuss whether MBE can provide lower disorder materials in the GeSn-Si system compared to those devices fabricated from chemical vapour deposition wafers [1, 2]. High levels of disorder are possibly a universal characteristic of present GeSn devices and the aims of this research are: (1) determine the carrier density from the Hall effect in the transport regime where the conductivity is thermally activated and discuss the experimental problems associated with this type of measurement. (2) determine if a Variable Range Hopping (VRH) transport regime is present at high p-type densities. In particular, do these devices enable us to understand why the transport mobility is activated and not the carrier density? (3) selectively etch devices to achieve a degree of thermal isolation with reduced influence of the thermal bath on the transport properties. This would be relevant for a Many Body Localization (MBL) based investigation and generally for future devices where a degree of thermal isolation is a requirement. (4) determine if surface segregation of β-Sn during the growth of the wafers influences the electrical properties of the subsequent devices and can high Sn content GeSn wafers be grown by MBE?

In this paper we present the electrical transport properties of GeSn Quantum wells. In section 2 the wafers are described in addition to the types of transport measurement involved. Section 3 is a summary of the electrical transport data. Section 4 is a discussion and comparison to RP-CVD (reduced pressure-chemical vapour deposition) material wafers and in section 5 conclusions are made with suggestions for further study of this important electronic material. The rest of the introduction describes further background information on GeSn growth, wafers and devices.

High Sn content GeSn quantum wells with high Sn content barrier layers are predicted to stabilize topologically protected surface states [3]. This presents a formidable technological challenge as Sn incorporation is limited to ~ 1% in Ge under normal *bulk* growth conditions. To achieve higher Sn content, non-equilibrium growth conditions are required with Sn levels of ~ 10% achievable [4]. This level of Sn incorporation is too low for the predicted topologically protected surface states but does lead to a direct band gap in the GeSn quantum well. An unavoidable strain is present due to the growth on Ge and the compressive strain in the $Ge_{0.90}Sn_{0.10}$ alloy tends to produce a minimum band gap at the L-point of the conduction band reversing the effects of Sn alloying [5]. Metastable Sn-rich phases generally need low growth temperature irrespective of whether MBE or RP-CVD is used [6]. In-situ TEM (Transmission Electron Microscopy) [7] combined with heating experiments have identified different Sn decomposition (mainly segregation) modes. This is not just important for growth of high mobility/quality GeSn structures but also provides thermal budget limitations to device fabrication-particularly for dielectric layer deposition and ohmic contact annealing. The thermal stability of MBE grown $Ge_{1-x}Sn_x$ was studied to optimise device quality material with surface segregation again the main technical issue [8]. Although there are problems associated with electrical quality in GeSn substantial progress has been made on fabricating structures at the nanoscale [9, 10].

The modulation doped GeSn quantum well system has been predicted to behave with a high mobility for both electrons and holes when strain is considered [11] and indeed this is manifest as a high single particle or quantum mobility [1] in the case of the two-dimensional (2D) hole gas. What was not predicted in [11] was the thermally activated transport mobility that is characteristic of this material [2]. This results from the disorder due to Sn segregation in the surface region that is due to this low solubility of Sn in the Ge lattice. The material discussed in [1] was grown by RP-CVD which for the p-Ge/GeSi system can produce hole gases with

mobility $> 4 \times 10^6$ cm^2/V.s [12]. What prevents this level of mobility in the GeSn quantum well system and can MBE growth technology be used to improve the electrical quality?

In the MBE growth of Ge$_{1-x}$Sn$_x$ quantum wells, see figure 1(a) for the wafer structure, the inefficient Sn incorporation can be manifest as a metallic β-Sn layer on the surface of the wafer. This can be due to a higher than optimal growth temperature [13]. The band offsets in this combination of material tends to stable carrier confinement in the GeSn valence band with B-modulation doping providing the charge carriers. The surface layer of the wafer can contain Sn in the metallic β-phase. This has a bulk superconducting transition (T_c) temperature of 3.8 K [14] and can be dilute enough not to influence the underlying electrical properties of the quantum well. In fact it may aid ohmic contact formation [15] or be incorporated as a highly transmissive superconducting ohmic contact in a hybrid device. In [15] it was reported that Sn-segregation at a Ti/Ge$_{0.95}$Sn$_{0.05}$ contact reduced the specific contact resistivity by a factor of 4. However considering these advantages, the Sn surface layer can introduce other issues that are discussed further in the paper such as providing a parallel conduction path in the device or expelling magnetic flux if Sn is in the superconducting phase.

1.2. Introduction to localization

The levels of disorder are generally very high in GeSn devices grown by RP-CVD [1, 2] and electrical transport mechanisms are dominated by thermally activated transport processes. This regime of transport can also be described by a percolation of the conductivity in the device and an indicator of this is the critical carrier density for the percolation threshold (non-zero) conductivity at low temperature. Previous measurements [16] in this transport regime on Si-based MOSFETs (metal oxide semiconductor field effect transistors) identified a gate tunable mobility edge with a transition to VRH conductivity for the case of disordered Si-based devices. In [17] localization was seen in a Si p-MOSFET for hole carrier densities $< 1.2 \times 10^{12}$ cm^{-2} due to confining potential fluctuations. This was presented as a percolation problem at the time and is considered further in section 4 in relation to GeSn devices. The Hall effect has been difficult to measure at the percolation threshold, although some measurements have been reported [18] close to the Metal-Insulator-Transition. A Coulomb gap at the chemical potential in the hopping transport regime has been identified in Si [19] and in GaAs/AlGaAs devices [20], a transition in the VRH between Mott (single particle hopping) and Efros-Shklovskii (an induced Coulomb gap) mechanisms can be observed. A more detailed discussion on Variable Range Hopping behaviour is presented in section 4. Disordered GeSn devices contain a key ingredient for the manifestation of Many Body Localization [21] with some of the experimental issues relating to this discussed in section 4.

2. Methods

The wafers of Ge$_{0.91}$Sn$_{0.09}$ were grown using MBE on undoped (001) Si substrates. Table 1 is a summary of the properties of the four Ge$_{0.91}$Sn$_{0.09}$ wafers that were measured in this work. This complements figure 1(a) showing a typical wafer structure cross-section. Recent work [22] carried out in the same MBE chamber has outlined how post growth annealing can influence the structural and electrical properties of GeSn devices and this was implemented in this study to improve the electrical quality of the wafers. In fact, post-growth annealing of wafers 3 was used in this study and the properties are discussed in further sections. These structures were nominally intended to be higher mobility, modulation doped structures. The p-type doping is provided by boron (shallow) acceptors at the level of 10^{17} to $\sim 10^{18}$ cm^{-3} density. The measured two-dimensional carrier densities are $\sim 10^{12}$ cm^{-2}, see table 1. The modulation doping is offset by 20 nm from the quantum well and this proximity does not influence the disorder potential at the quantum well. The disorder that is evident in the electrical measurements is a result of Sn segregation during the MBE growth.

wafer	roughness (1) (rms nm) ± 0.05 nm	Ge buffer layer (μm)	post-growth anneal (2)	modulation doping density (cm^{-3})	measured Hall density (cm^{-2}) (3)
1	1.5 - 2.2	1.1	not-annealed	1.2×10^{18}	2.2×10^{13}
2	edge: 1.05 [figure 1(b)] centre: 1.9	2.0	not-annealed Sn-segregation	2×10^{17}	0.4×10^{12} to 2.5×10^{12}
3	edge: 0.89	3.0	annealed	1×10^{17}	1.3×10^{12}
4	edge: 0.63 - 0.91	3.0	not-annealed	1×10^{17}	3.3×10^{12}

(1) Atomic force microscopy (AFM) measurements. rms refers to root-mean-square calculated values. The edge is the outer edge of the 2-inch wafer and centre refers to a 7×7 mm region in the centre of the 2-inch wafer. (2) Anneal conditions (reducing the carrier density): annealed at 130°C [7, 23]. (3) Mean Hall effect sheet density at low temperature, determined over a set of devices. P-type behaviour is due to B doping and band offsets in the valence bands of Ge-GeSn for hole confinement.

Table 1. A summary of the growth and physical properties of the wafers measured in this study.

Initial measurements were made on Van der Pauw (VdP) devices (consisting of 3×3 mm squares) [24] with low temperature, annealed indium ohmic contacts (~ 150°C) for rapid device assessment. Standard Hall bars for electrical transport measurements were then cleanroom fabricated from each wafer. A wet etch consisting of $HCl:H_2O_2:H_2O$ (1:1:20) was used to define the mesa. Thermally evaporated aluminium was used as an ohmic contact after a rapid thermal anneal at 250°C. The suspended devices were fabricated by selectively etching a Si layer below the Ge-buffer layer. This can be done either by dry etching [25] with a Si:Ge etch ratio of 70:1 or with NH_4OH-based selective etchants [26, 27]. This technology is now being developed with Si-rich buffer layers incorporated during growth below the active part of the device, see figure 1. Although this was an initial goal of the work, the transport measurements that are presented in this publication are from the non-suspended devices.

Electrical transport measurements of resistivity components (ρ_{xx} and ρ_{xy}) were made initially down to 1.5 K with magnetic fields up to 8 T. A Triton dilution refrigerator was also used for measurements from ~ 1 K to 30 mK where the conductivity in the localization regime can be accessed. Standard four-contact, ac current excitation using lock-in amplifiers and voltage pre-amplifiers were used initially. In the localization regime (lower carrier density, lower temperature) two-contact, dc voltage excitation was used with a Keithley model 6430 sub-femtoamp remote source meter. Several devices were measured multiple times in different cool downs and in different measuring systems; this is indicated in the relevant tables and figures.

3. Results

3.1. A summary of the GeSn wafers

Starting with a general overview of the MBE wafers: Wafer 1 was parallel conducting due to the intentionally high, modulation doping density. This high doping density is needed in the case of suspended devices where there is a significant reduction in the carrier density in the quantum well when a new surface below the quantum well is formed through a selective etching process. Introducing controlled focussed ion beam (FIB) damage to the quantum well region (utilizing Ga$^+$ ions at 30 keV with a dose of 6.7×10^{10} ions/cm^2) did not change the measured conductivity demonstrating that parallel conduction was present in the devices below the quantum well, see table 2 for a summary. Dark and light electrical measurements (using an

in-situ LED) are very similar indicating that the doping is fully activated, even in dark conditions at low temperature. This high carrier density in wafer 1 is unlikely to be only charge confined to the quantum well as that would have been sensitive to illumination levels due to a persistent photoconductivity effect. Table 2 is a summary of the electrical properties of wafer 1, including the FIB damaged devices.

wafer 1 devices Hall bars	resistivity (Ω/sqr)	p (cm^{-2}) (2)	μ (cm^2/V$\times$s) (3)
c(1)	725$\pm$50	--	--
c(1) FIB damaged (1)	715$\pm$38	--	--
c(2)	540$\pm$14	2.2$\times$10^{13}	540
c(2) FIB damaged	540$\pm$16	2.2$\times$10^{13}	520

(1) FIB damage parameters: 30 keV, dose 6.7$\times$10^{10} ions/cm^2. (2) p is the hole carrier density from the Hall effect. (3) μ is the characteristic mobility. c refers throughout this paper as chip number, chip(1) as c(1) for example. sqr refers to the number of squares of material on the mesa between voltage probe contacts.

Table 2. The electrical properties of devices from wafer 1 at 1.5 K.

Wafer 2 had a thicker Ge buffer layer (this reduces the measured surface roughness) and a lower modulation doping density. Figure 1(b) shows an AFM image of wafer 2 from the edge region. The roughness is 1.05 nm over an area of 20x20 μm. The measured hole density was 1.5$\times$10^{12} cm^{-2} with a mobility of 200 cm^2/V.s at 4 K albeit after a brief illumination. This can produce a persistent photoconductivity effect in this type of device [2] although this was not apparent in wafer 1. Table S1 in the supplementary section summarises the devices fabricated from wafer 2. The Van der Pauw devices (3) to (5) with non-annealed Ag epoxy contacts showed diodic behaviour at 77 K. This indicates that there is no continuous β-Sn layer in the surface region. If a continuous metallic β-Sn layer were present and covering the surface then an Ag epoxy contact would have made a non-annealed ohmic contact. In table S1, the carrier densities from the Van der Pauw devices are consistently lower than that from the Hall bars, this is a real effect and is discussed in further sections below. Wafer 3 was annealed during the growth process and devices fabricated from this wafer are summarised in table S2. These devices from wafer 3 had a consistently higher mobility due to the reduction in alloy disorder close to the quantum well as a result of the optimized annealing conditions.

3.2. Mobility and carrier density from the Hall effect

Figure 2 shows the temperature dependence of the mobility (a) and carrier density (b) in the range of devices fabricated from wafer 2. At low temperature the carrier density is independent of temperature. At carrier densities larger than $\sim 2\times10^{12}$ cm^{-2} there is an influence of parallel conduction which provides an extrinsic carrier density that is temperature dependent, this is clear in figure 2(b) at temperatures > 6 K. The variation in carrier density is due to devices from different parts of the wafer having different levels of activated doping and disorder; this is partly due to a growth temperature variation across the wafer during the MBE growth. The mobility is strongly temperature dependent in a way that was also observed in RP-CVD material [1]. The temperature dependent mobility, μ(T) can be described by equation (1) where μ_o is the high temperature mobility and T_o is the characteristic temperature associated with the activated behaviour between the chemical potential and the mobility edge in the valence band density of states,

$$\mu(T) = \mu_o e^{-(\frac{T_o}{T})} \tag{1}$$

6

$k_B \times T_o$ is the activation energy to the mobility edge in the GeSn valence band, k_B is Boltzmann's constant. In figure 3 the mobility of devices from wafer 2 are plotted against inverse temperature, $1/T$. The Hall mobility has been determined from $\mu = \sigma \times R_H$., where R_H is the Hall constant from the Hall effect and σ is the conductivity at zero magnetic field. A typical range of T_o values from fitting equation (1) are 10 K to 15 K although the least square fits are not shown in the plot. The temperature dependence of the mobility in figure 3 does not fit to a power law dependence. This rules out a quasi-3D (three-dimensional) ionized impurity scattering limit mobility where $\mu \sim T^{0.5}$ would be expected for extrinsic carrier behaviour. A power law plot is shown in the supplementary section, see figure S1, with a $\sim T^2$ dependence developing at higher temperatures.

The Hall effect is difficult to quantify in the regime where the conductivity is thermally activated. This is discussed further in section 4 after the experimental data is presented here. Figure 4 shows the Hall resistance in devices from wafer 2 and wafer 3 over a range of temperatures in the region of $\rho_o >> \rho_{xy}$, where ρ_o is the measured zero magnetic field resistance. In wafer 3 the transverse Hall voltage (at 3 T) is ~ 0.6 % of the longitudinal resistance signal at 2.57 K for device Hall bar c(2), see figure 4(b). The dotted lines are second-order polynomial fits with the additional B^2 component fit that is due to the inadvertent mixing of ρ_o into ρ_{xy} that has not been completely removed from the component of ρ_{xy} by averaging over positive and negative fields. The B linear component gives a carrier density, $p = 3.6 \pm 1.1 \times 10^{12}$ cm^{-2} from a least squares fitting procedure. The error bar (for p) represents a change in the field domain for the ρ_{xy} fit between 0 and 1 T to between 0 and 3 T in steps of 0.5 T in the upper field value. The Hall effect signal is difficult to quantify in a systematic way irrespective of the random noise levels in the signal. The main experimental difficulty is temperature stability when the ρ_{xx} signal is thermally activated and the ρ_{xy} signal is independent of temperature. The temperature problem is a drift in temperature over the course of the measurement ($\sim$30 minutes), with $\pm$ 0.1 K enough to cause variations in ρ_{xx} that are comparable in size to the ρ_{xy} signal. In figure 4(b) the difference in set temperature is 0.14 K but this results in a significantly different Hall signal; $\sim$10% difference in the carrier density. It is easier to remove components that scale as B^2 from a Van der Pauw measurement; this then gives a better representation of ρ_{xy}. In fact non-optimal removal of B^2 components results in a reduction in ρ_{xy} and a correspondingly higher apparent carrier density in the Hall bar devices.

3.3. Temperature dependent conductivity

The measured carrier density from the Hall effect is between 0.5 and 2.5×10^{12} cm^{-2} in the GeSn MBE material at 4 K with the devices showing the characteristics of a mobility edge at lower carrier densities. In this regime the conductivity is described by equation (2),

$$\sigma(T) = \sigma_o e^{-\left(\frac{T_o}{T}\right)} \tag{2}$$

where T_o is a characteristic temperature relating to the energy difference in the density of states between the chemical potential and the mobility edge. The actual energy would be $k_B \times T_o$. With constant carrier density the behaviour of the conductivity is identical to that of the mobility described by equation (1). In figure 5(a) the conductivity in Hall bar c(2) device from wafer 2 is plotted as a function of $1/T$. The measured carrier density is 2.2×10^{12} cm^{-2} and is also shown in figure 2(a). The conductivity down to 1.5 K is not thermally activated in this case. The subset of red data points are included a fit to equation (2) with the $T_o \sim 1$ K lower than the actual measurement temperature. The conductivity could be activated at lower temperatures but there is only one experimental data point at ~ 1 K with conductivity $0.080 \pm 0.001 \times (e^2/h)$.sqr. At lower temperatures (< 700 mK) this device is too resistive to measure using small ac signal response and out-of-phase components start to dominate the measured voltage signals. Figure 5(b) shows the conductivity in Hall bar c(3) device from wafer 2 with a carrier density of

1.5×10^{12} cm^{-2}. The conductivity is thermally activated from ~ 1 K with $\sigma_o \sim 1.5 \times (e^2/h)$.sqr and $T_o \sim 3$ K, which is above the actual measurement temperature. The intercept in conductivity is close to the well-defined Mott minimum metallic conductivity in GeSn devices [2], although further gated measurements are needed to confirm this in the MBE material. This is occurring at a higher hole carrier density, typically ~ 1-2×10^{12} cm^{-2} compared to 1.6×10^{11} cm^{-2} in RP-CVD materials. The experimental data in figure 5 is taken using the four-contact ac current excitation and conductivities as low as $\sim 0.028 \times (e^2/h)$.sqr can be measured. The unwanted capacitive part of the measured signal dominates the small ac excitation signal, below ~ 900 mK.

To measure devices in the lower temperature regime, the two-contact configuration was used and a change over to a VRH conductivity could be seen in the wafer 2 Hall bar c(3). The contribution to the conductivity of the device in this regime is given by equation (3),

$$\sigma(T) = \sigma_o e^{-\left(\frac{T_o}{T}\right)^q} \tag{3}$$

where q is the power relating to the details of the VRH transport (q = 1/2 or 1/3 depending on Mott [28] or Efros-Shklovskii [29] VRH mechanisms) and σ_o takes on quantised values relating to (e^2/h).sqr, $\times 2$ for Mott and $\times 1$ for Efros-Shklovskii that enable the type of VRH to be determined. The details of this are discussed further in section 4. Measurements in this region of conductance are into the strongly localized regime where reliable Hall measurements are not available and the small ac signal method is not reliable. The only data available is the conductance obtained by applying a small dc voltage and measuring the current in a two-contact configuration. The Keithley model 6430 sub-femtoamp remote source meter can measure down to ~ 10 fA in this experimental set-up. In figure 6(a) we show this type of experimental data taken on device Hall bar c(3) from wafer 2. The lowest measurement temperature is 50 mK, although on the (linear) scale of current (I) shown in figure 6(a) there is no finite current visible until ~ 0.2 K. Below this temperature, the conductance is non-linear. The red dotted lines (at applied voltage ± 0.05 V) show the regions of applied voltage (V) where a unique linear conductance can be determined. In figure 6(b) the conductance (G = I/V) is plotted as a function of $T^{-0.5}$ showing a Coulomb gap behaviour with temperature. The red line is a least squares fit to equation (3) with q = 1/2. The fit is linear over more than four orders of magnitude in experimentally determined G with a conductance intercept of $4.5 \times (e^2/h)$ and a characteristic T_o of 55 K. The conductance intercept is higher than the conductivity intercept for Efros-Shklovskii VRH (typically e^2/h) due to not taking into account the geometry of the device.

In the GeSn material system the hole-phonon coupling strength is relatively strong as there are no current-voltage jumps with small applied dc voltage, i.e. the hole temperature is strongly connected to lattice temperature even for applied voltages where non-linear behaviour would be expected. In comparison to disordered InSb devices, the charge-phonon coupling strength is $\times 100$ stronger in GeSn [30]. In applied magnetic fields the conductance can be still described by equation (3) with the characteristic T_o depending weakly on B, in fact $T_o \sim \log_{10}(B)$ from field dependent measurements. There is no screening of the Efros-Shklovskii VRH mechanism caused by metallic β-Sn in the device and the hole localization length estimated from the Efros-Shklovskii characteristic temperature T_o is ~ 65 nm in this material.

3.4. Percolation of the conductivity

The characteristic carrier density where the conductivity tends to zero at low temperature is an important parameter, the percolation density (p_c). This can give critical information on the device potential with intrinsic levels of disorder, for example in the recent high mobility, modulation doped p-Ge system, p_c can be as low as 0.5×10^{10} cm^{-2} [12]. The

percolation density is determined by fitting σ as a function of p at low (constant) temperature, see equation (4),

$$\sigma(p) = \alpha(p - p_c)^\beta \qquad (4)$$

where β is the power exponent and α is the prefactor. Equation (4) is valid for $p > p_c$. In figure 7 we plot σ as a function of p for several devices from wafer 2. In this plot, p is determined from the measured Hall effect not a gate voltage and calibrated gate capacitance. The quality of the data is not sufficient to determine the characteristic parameters α and β with this data set as there is a variation in temperature in the measured data and α, β can be temperature dependent. A gated device will be more appropriate for a detailed determination of these parameters. Further device development will address this issue assuming that Sn segregation does not screen the gate potential or cause leakage paths through the device. In the GeSn devices reported here, the percolation density is $\sim 1.0\pm0.5\times10^{12}$ cm^{-2} substantially higher than that recently reported in p-Ge devices [12].

4. Discussion

4.1. The Hall effect in GeSn devices

In section 3 we presented Hall effect measurements in the region where the device conductivity is thermally activated. This causes experimental problems for determining the actual Hall effect signals in the region of charge localization [18]. Experimentally the Hall voltage is analysed using equation (5)

$$\rho_{xy}(B) = 0.5 \times [\rho_{xy}(+ B) - \rho_{xy}(-B)] \qquad (5)$$

to get a more representative ρ_{xy} signal. This works when there is a *moderate* contribution to ρ_{xy} from ρ_{xx}. This mixing of resistivity components is partly due to the processing of the Hall bar that ideally ensures parallel current contours and opposed ohmic contacts. There is an additional, more fundamental problem [18] and this reference discusses the contribution of spin-orbit coupling to the Hall constant with spin-orbit coupling known to be operating in GeSn devices [31]. This problem could occur in GeSn devices even before the transport mechanism switches to VRH.

It is the resistance R_{xx} (not resistivity) that can add to ρ_{xy} and in the case of the VdP geometry this resistance is $\rho_{xx}\times\ln2/\pi = 0.22\times\rho_{xx}$ whereas in the Hall bar this resistance is $\rho_{xx}\times(L/W) = 9.30\times\rho_{xx}$ where L and W are the length and width of the mesa between voltage probe contacts used for ρ_{xx}. This gives a factor of 42 difference in the resistance that can (in principle) mix into ρ_{xy} depending on the device asymmetry with the Hall ohmic contacts. This factor is due to the non-parallel current contours in the case of the VdP device. Hence, the Van der Pauw device should allow Hall measurements further into the localization regime or at least to lower temperatures. In practice, it tends to be device processing that determines how much the ρ_{xx} and ρ_{xy} signals are mixed. Generally this method of using equation (5) is sufficient until $\rho_{xx} \sim h/e^2$, 25.8 kΩ then conductance fluctuations (as a result of variations in T) start to be dominant and the ±B averaging comes less effective in removing ρ_{xx} related signals, see figure 4(a) when $\rho_o \sim 40$ kΩ. There are other semiconductor device systems that show the effects of localization and table 3 below summarises the measured carrier density in the localization regime in these other devices.

device	carrier density (cm^{-2})	conductivity	reference
p-GeSn quantum well (RP-CVD growth)	p-type 4.4×10^{11}	mobility gap	[1]
p-Si MOSFET	p-type 1.2×10^{12}	mobility gap	[17]
n-Si MOSFET	n-type 1.0×10^{12}	Mott 2D VRH	[32]

Table 3. The measured low temperature carrier density in several device schemes that show the effects of localization.

An added complication exists for the case of Sn segregation in GeSn devices. A β-Sn layer would expel magnetic flux (in the superconducting state up to ~ 2.5 T) and influence the Hall signal in these measurements made typically below the 2.5 T critical magnetic field. Also surface β-Sn could shunt the applied current or locally short the Hall voltage even if the β-Sn is not a continuous layer. However, screening of the Coulomb interaction in the devices does not appear to be operating in GeSn with significant β-Sn segregation. The main practical problem for β-Sn segregation is processing related and this effect reduces the reliability of gating structures for 2D carrier density modulation or quantum structure fabrication through depleting surface gates.

4.2. The conductivity in GeSn devices

The conductivity observed in figure 5 represents the on-set of a mobility gap in the region of $p \sim 2\times10^{12}$ cm^{-2}. The activated behaviour shows a mobility gap in figure 5(b) in the region of ~1 K. This agrees with that observed previously in the behaviour of RP-CVD devices [2], particularly relating to the conductivity intercept. In [2] the conductivity intercept reduces to $0.12\times(e^2/\hbar)$, with $\hbar$ Planck's constant divided by 2π, at lower carrier density and this observation is close to the accepted Mott Minimum Metallic conductivity value. Although this is now considered a concept, it manifests itself as clear limit in GeSn. It does not work at very low temperatures but is accurate at higher when the phase coherence length is smaller or of the order of the elastic scattering length so that the quantum interference due to backscattering is not significant. The main development that is reported in this paper is the transition to a VRH conductivity that was absent in the RP-CVD based devices. This transition occurs below ~ 1 K and is only clearly observed using the two-contact conductance measurements reported in section 3.3 and shown in figure 6. The Efros-Shklovskii mechanism can in principle be screened by a metallic gate, although in the devices reported here there is no surface gate only a potential β-Sn layer due to surface segregation during the MBE growth process. In fact, the Efros-Shklovskii mechanism is screened by a metal gate when the characteristic hopping length is ×2 the distance of the 2D system from the surface gate [20]. Possible segregation does not screen any Coulomb interactions at least with a nominal Ge$_{0.90}$Sn$_{0.10}$ layer. This may be one advantage of the MBE growth method and be attractive to the higher Sn compositions where topological states have been predicted to dominate the band structure [3]. There are several transport mechanisms in the VRH regime,

conductivity type	conductivity prefactor	exponential power law	comment:
Drude (1)	$(k_f\times l_e)\times$sqr	T^0	k_f : Fermi wave-vector, l_e : elastic mean free path
mobility edge	$0.1\times(e^2/\hbar)\times$sqr	$-(T_o/T)^1$	$p = 1.6\times10^{11}$ cm^{-2} [2]
Mott 2D VRH (2)	$2\times(e^2/h)\times$sqr	$-(T_o/T)^{1/3}$	2D system [28]
Efros-Shklovskii VRH	$(e^2/h)\times$sqr	$-(T_o/T)^{1/2}$	[29] (2D and 3D systems) upper bound on p due to screening
Power Law Hopping	---	power law in T	[33]
Many Body Localization (MBL)	---	---	[34] no thermal bath connection

(1) Non-thermally activated $\sigma = (k_f \times l_e) \times (e^2/h)$. (2) This Mott VRH is for a 2D geometry. Generally for the Mott mechanism, the power $q = 1/(d+1)$ where d is the dimensionality of the system.

Table 4. A summary of several behaviour types of the conductivity in the localised regime.

and table 4 summarizes these mechanisms although the list here is not exhaustive. The necessary condition for thermal isolation needed to observe an MBL state is more promising in GeSn devices as the conductance at higher carrier densities behaves as if there is a mobility edge not a VRH dominated transport regime. The lattice temperature at which a bistability can be seen in the electron temperature (due to current over-heating effects) is then in an experimentally accessible range. In the case of VRH (both Mott and Efros-Shklovskii mechanisms) the characteristic temperature for decoupling of the hole-phonon interaction would be below the base temperature of most dilution refrigerators. This is discussed further [21] where the large hole-phonon coupling strength in GeSn does mean though that the voltage required to over-heat the hole gas is comparatively large. Any large applied voltage is likely to contribute to competing transport mechanisms such as impact excitation, impact ionization and field enhanced hopping. A thermally isolated Hall bar is also a requirement for observation of MBL and processing developments will ensure that this type of device is available for transport measurements. Recent progress in this respect is presented in the supplementary section.

The role played by hole spin has not been discussed in this work although there are reports that spin-orbit coupling exists in GeSn based devices [31]. In fact, in disordered systems the spin lifetime can be enhanced due to the D'yakonov-Perel dominant spin relation mechanism where the spin relaxation rate is proportional to the momentum scattering mean free time. A weak antilocalization (WAL) effect due to spin-orbit coupling has been identified in GeSn devices [31] with a very short, characteristic spin relaxation length of 20 to 30 nm. However, there is no positive magnetoresistance observable in the MBE grown wafers and devices reported in this publication that could be attributed to WAL, and this may come down to the details of epitaxial strain in the wafers or the overall asymmetry of the confining potential.

5. Conclusions

We have reported the electrical transport properties of devices from four MBE grown $Ge_{0.91}Sn_{0.09}$ quantum well wafers. A high level of disorder exists in MBE grown epitaxial GeSn that is fundamentally due to segregation of β-Sn during growth with residual β-Sn incorporated into the surface regions in non-optimized wafers. The p-type quantum well devices show evidence for a mobility edge with a thermally activated conductivity and 2D hole densities as high as 2×10^{12} cm^{-2}. We have discussed measuring the Hall effect in this experimentally difficult region where the conductivity shows activated behaviour resulting in the Hall resistance < 1% of the longitudinal resistance. The measured percolation hole density in MBE modulation doped GeSn is in the region of $\sim 1 \times 10^{12}$ cm^{-2}, although surface gated measurements are needed to confirm this high level. In the four-contact ac measurements, conductivities as low as $\sim 0.028 \times (e^2/h)$.sqr were measured showing the characteristic behaviour of a mobility gap. This behaviour is also observed in GeSn grown by RP-CVD and maybe a universal property of Ge/GeSn devices. At temperatures < 1 K the presence of a Variable Range Hopping mechanism showing a Coulomb gap was determined using dc transport, constant voltage measurements in the two-contact configuration. Conductances as low as $\sim 10^{-6} \times (e^2/h)$ were able to be accurately measured. The surface segregated β-Sn does not influence the transport measurements in terms of expelling magnetic flux (in the superconducting phase) or screening carrier interactions in the quantum well region. This will be useful for future quantum devices

and will lead onto devices that operate on the principles of topologically protected surface states if higher Sn compositions can be incorporated into the quantum well and barrier regions.

Data availability statement
The complete experimental data set from this programme of work will be available on Zenodo https://zenodo.org/ when the manuscript is accepted.

Declarations
Conflict of Interest The authors have no-conflicts of interest to disclose.

References

[1] Gul Y, Myronov M, Holmes S N, and Pepper M 2020 Activated and Metallic Conduction in p-Type Modulation-Doped Ge-Sn Devices *Phys. Rev. Appl.* **14** 054064

[2] Gul Y, Holmes S N, Cho Chang-Woo, Piot B, Myronov M, and Pepper M 2022 Two dimensional localization in GeSn *J. Phys.: Condens. Matter* **34** 485301

[3] Ferrari B M, Marcantonio F, Murphy-Armando F, Virgilio M, and Pezzoli F 2022 Quantum spin Hall phase in GeSn heterostructures on silicon *arXiv*:2210.0298

[4] Kasper E, Werner J, Oehme M, Escoubas S, Burle N, and Schulze J 2012 Growth of silicon based germanium tin alloys *Thin Solid Films* **520** 3195

[5] Wirths S, Buca D, Mantl S 2016 Si-Ge-Sn alloys: From growth to applications *Progress in Crystal Growth and Characterization of Materials* **62** 1

[6] Jahandar Pedram 2022 Low-temperature heteroepitaxy of $Ge_{1-y}Sn_y$ binary alloy using chemical vapor deposition APS March Meeting 2022 abstract id.T00.295

[7] Martinez Kari, Minenkov Alexey, Aberl Johannes, Buca Dan, Brehm Moritz, and Groiss Heiko 2023 *In situ* TEM heating experiments on thin epitaxial GeSn layers: Modes of phase separation *Appl. Phys. Lett. Mater.* **11** 101117

[8] Lemire Amanda N, Grossklaus Kevin A, Vandervelde Thomas E 2023 Variation in thermal stability of $Ge_{1-x}Sn_x$ films for infrared device applications *J. Vac. Sci. Technol.* A **41** 052701

[9] Gupta Suyog, Chen Robert, Huang Yi-Chiau, Kim Yihwan, Sanchez Errol, Harris James S, and Saraswat Krishna C 2013 Highly Selective Dry Etching of Germanium over Germanium-Tin $(Ge_{1-x}Sn_x)$: A Novel Route for $Ge_{1-x}Sn_x$ Nanostructure Fabrication *Nano Lett.* **13** 3783

[10] Doherty Jessica, et al 2020 Progress on Germanium-Tin Nanoscale Alloys *Chem. Mater.* **32** 4383

[11] Sau Jay Deep, Cohen Marvin L 2007 Possibility of increased mobility in Ge-Sn alloy system *Phys. Rev. B* **75** 045208

[12] Myronov Maksym, Kycia Jan, Waldron Philip, Jiang Weihong, Barrios Pedro, Bogan Alex, Coleridge Peter, and Studenikin Sergei 2023 Holes Outperform Electrons in Group IV Semiconductor Materials *Small Sci.* 2200094 DOI: 10.1002/ smsc.202200094

[13] Weisshaupt D, Jahandar P, Colston G, Allred P, Schulze J, Myronov M 2017 Impact of Sn segregation on $Ge_{1-x}Sn_x$ epi-layers growth by RP-CVD *MIPRO* (Opatija, Croatia, 22–26 May 2017) DOI: https://doi.org/10.23919/MIPRO.2017.7973388

[14] De Haas W J, De Boer J, Van den Berg G J 1935 The electrical resistance of cadmium, thallium and tin at low temperatures *Physica* **2** 453

[15] Wu Ying, Xu Haiwen, Han Kaizhen, and Gong Xiao 2019 Thermal Stability and Sn Segregation of Low-Resistance Ti/p$^+$-$Ge_{0.95}Sn_{0.05}$ Contact *IEEE Electron. Dev. Lett.* **40** 1575

[16] Pepper M, Pollitt S, Adkins C J, and Oakley R E 1974 Variable-Range Hopping in a Silicon Inversion Layer *Phys. Letts.* **47A** 71

[17] Arnold Emil 1974 Disorder-induced carrier localization in silicon surface inversion layers *Appl. Phys. Lett.* **25** 705

[18] Koon D W, and Castner T G 1990 Hall effect near the metal-insulator transition *Phys. Rev. B* **41** 12054

[19] Mason Whitney, Kravchenko S V, Bowker G E, and Furneaux J E 1995 Experimental evidence for a Coulomb gap in two dimensions *Phys. Rev. B* **52** 7857

[20] Khondaker S I, Shlimak I S, Nicholls J T, Pepper M, Ritchie D A 1999 Two-dimensional hopping conductivity in a δ-doped GaAs/Al_xGa_{1-x}As heterostructure *Phys. Rev. B* **59** 4580

[21] McArdle George, Lerner Igor V 2021 Electron-phonon decoupling in two dimensions *Scientific Reports* **11** 24293 DOI: https://doi.org/10.21203/rs.3.rs-885766/v1

[22] Jia Hui, Jurczak Pamela, Yang Junjie, Tang Mingchu, Li Keshuang, Deng Huiwen, Dang Manyu, Chen Siming, and Liu Huiyun 2020 Impact of ex-situ annealing on strain and composition of MBE grown GeSn *J. Phys. D: Appl. Phys.* **53** 485104

[23] Minenkov Alexey, Groiss Heiko 2021 Evolution of phases and their thermal stability in Ge-Sn nanofilms: a comprehensive *in situ* TEM investigation *J. Alloys and Compounds* **859** 157763

[24] van der Pauw L J 1958 A method of measuring specific resistivity and Hall effect of discs of arbitrary shape *Philips Research Reports* **13** 1-9

[25] Oehrlein G S, Bestwick T D, Jones P L, Corbett J W 1990 Selective dry etching of silicon with respect to germanium *Appl. Phys. Lett*. **56** 1436

[26] Wang Feng, Shi Yi, Liu Jianlin, Gu Sulin, and Zheng Youdou 1997 Highly Selective Chemical Etching of Si *vs.* $Si_{1-x}Ge_x$ Using NH_4OH Solution *J. Electrochem. Soc*. **144** L37

[27] Schnakenberg U, Benecke W, and Löchel B 1990 NH_4OH-based Etchants for Silicon Micromachining *Sensors and Actuator* **A21** 1031

[28] Mott N F 1968 Conduction in Glasses containing transition metal ions *J. Non-Crystalline Solids* **1** 1

[29] Efros A L, Shklovskii B I 1975 Coulomb gap and low temperature conductivity of disordered systems *J. Phys. C* **8** L49

[30] Gough J et al, unpublished 2024 Heating analysis shows the hole-phonon coupling constant in GeSn is $\sim 7.3 \times 10^{-8}$ $W \times K^{-5}$ for a 2D phonon dispersion

[31] Weisshaupt David, et al 2021 Weak Localization and weak antilocalization in doped $Ge_{1-y}Sn_y$ layers with up to 8% Sn *J. Phys.: Condens. Matter* **33** 085703

[32] Tsui D C, Allen S J 1974 Mott-Anderson Localization in the Two-Dimensional Band Tail of Si Inversion Layers *Phys. Rev. Lett*. **32** 1200

[33] Kaveh M 1985 Power-law localization in two-dimensional systems Theory and experiment *Philosophical Magazine* B **52** 521

[34] Nandkishore Rahul, and Huse David A 2015 Many-Body Localization and Thermalization in Quantum Statistical Mechanics *Annu. Rev. Condens. Matter Phys*. **6** 15

FIGURES

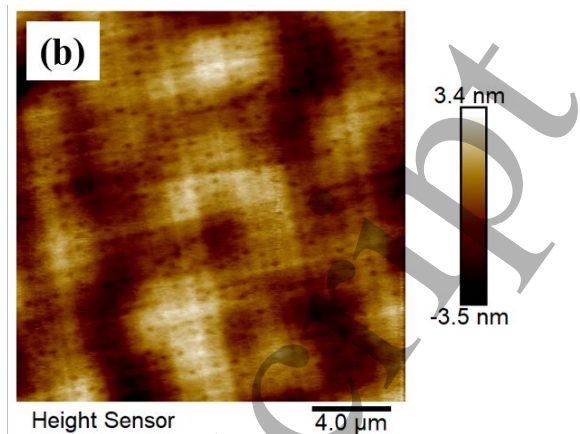| (a)	Ge cap	30 nm
	GeSn quantum well	15 nm
	Ge spacer	20 nm
	Ge (boron doped)	10 nm
	SiGe sacrificial layer	t_s nm
	relaxed Ge buffer layer	t_b μm
	undoped Si (001) substrate	

Figure 1. (a) The schematic cross section of a modulation doped $Ge_{0.91}Sn_{0.09}$ quantum well wafer, see table 1 for details. The variables between different wafers are the boron doping density and the thickness of the relaxed Ge buffer layer and the sacrificial layer. The p-type boron doping is offset by a 20 nm spacer from the quantum well. (b) An AFM image from the edge of wafer 2 showing a roughness of 1.05 nm across an area of 20x20 μm.
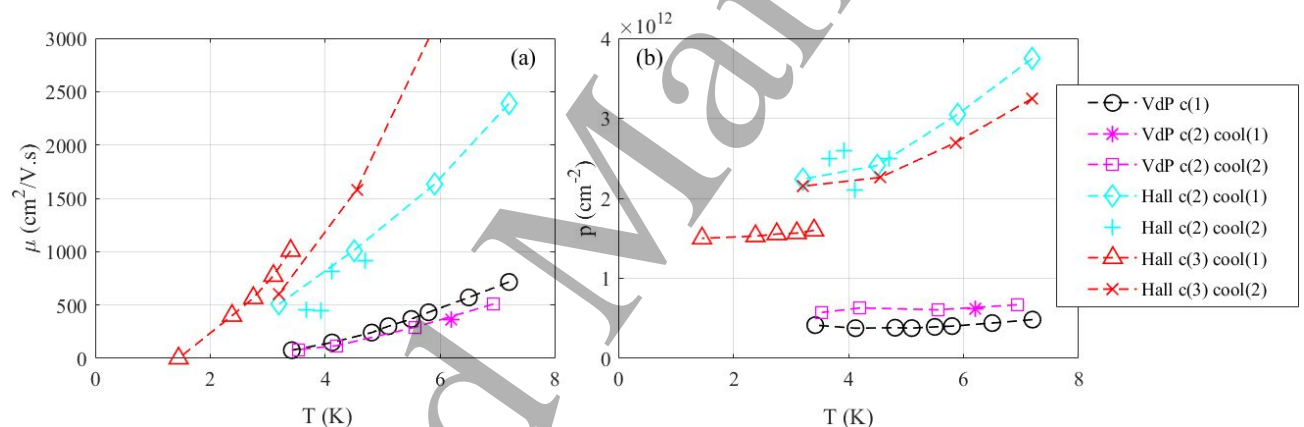
Figure 2. (a) The mobility (μ) and (b) hole carrier density (p) and from the Hall effect at low temperature for devices fabricated from wafer 2.
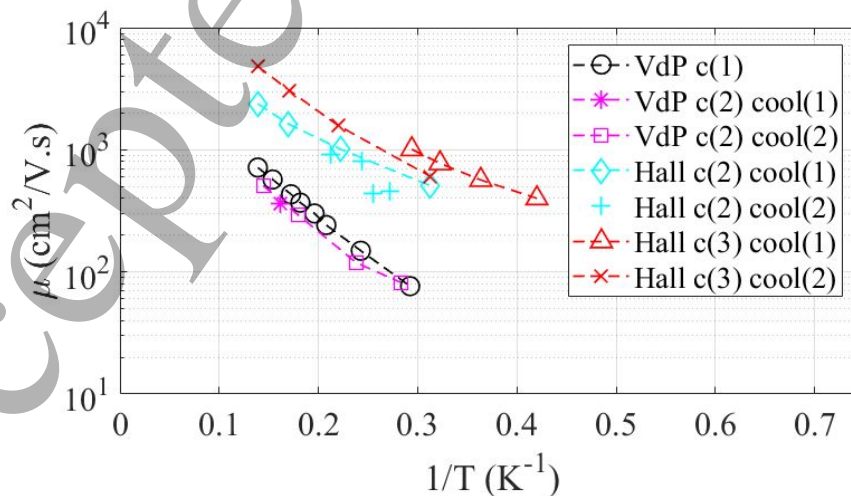

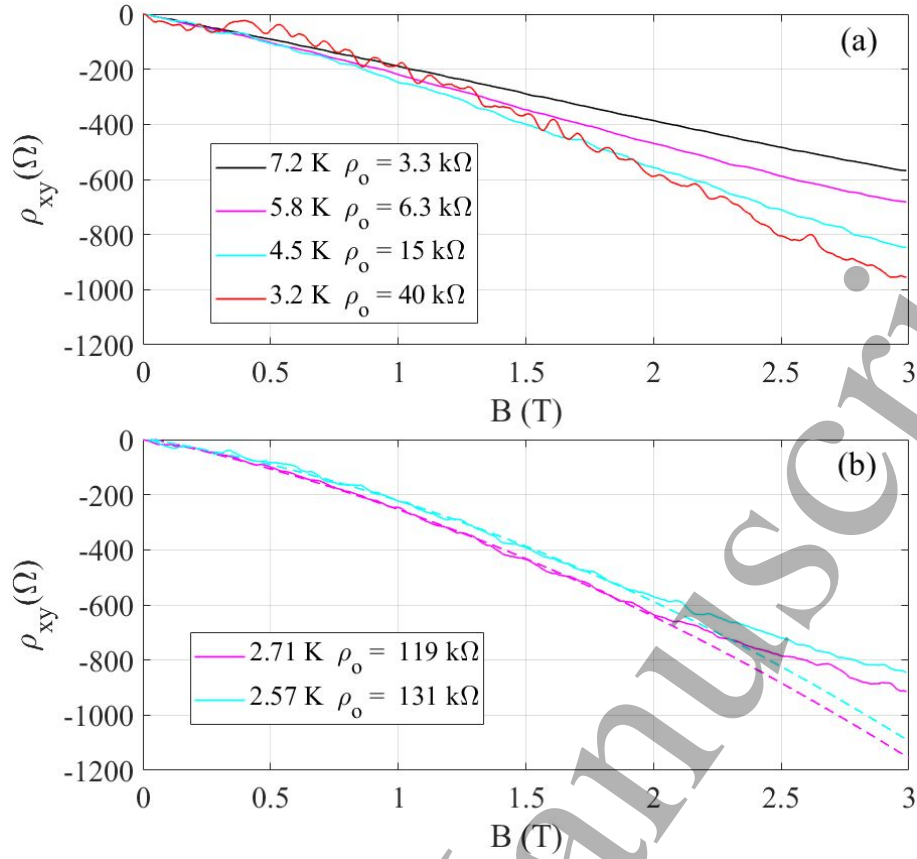**Figure 3.** The mobility as a function of 1/T for 4 different devices from wafer 2 measured from the Hall effect.

16

Figure 4. (a) The Hall resistance (ρ_{xy}) as a function of magnetic field (B) in device Hall bar c(3) from wafer 2 at temperatures from 7.2 to 3.2 K. ρ_o is the measured low magnetic field resistance (not resistivity) at zero field for comparison to the size of the Hall voltage, (b) The Hall resistance in device Hall bar c(2) from wafer 3. The dotted lines are second-order polynomial fits with the additional B^2 component fit that is due to the inadvertent mixing of ρ_{xx} into ρ_{xy} that has not been completely removed from the component of ρ_{xy}. This is discussed further in section 4.
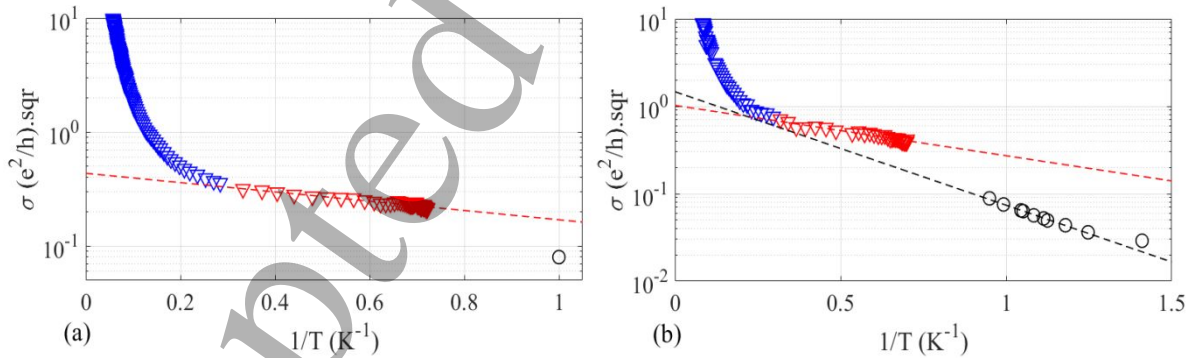

Figure 5. (a) The conductivity in Hall bar c(2) device from wafer 2 as a function of 1/T. The measured carrier density is 2.2×10^{12} cm^{-2}. The conductivity down to 1.5 K is not thermally activated and the T_o from a fit to equation (2) (the red data points) is lower than the measurement temperature. It could be activated at lower temperatures but there is only one data point at ~ 1 K with conductivity $0.080 \pm 0.001 \times (e^2/h)$.sqr. At lower temperatures (< 700 mK) this device is too resistive to measure using small ac signal response, (b) The conductivity in Hall bar c(3) device with a carrier density of 1.5×10^{12} cm^{-2}. The conductivity is thermally activated from ~ 1 K with $\sigma_o = 1.5 \times (e^2/h)$.sqr and $T_o = 3$ K, which is above the measurement temperature. The red and black data points correspond to cool downs in different cryostat systems.
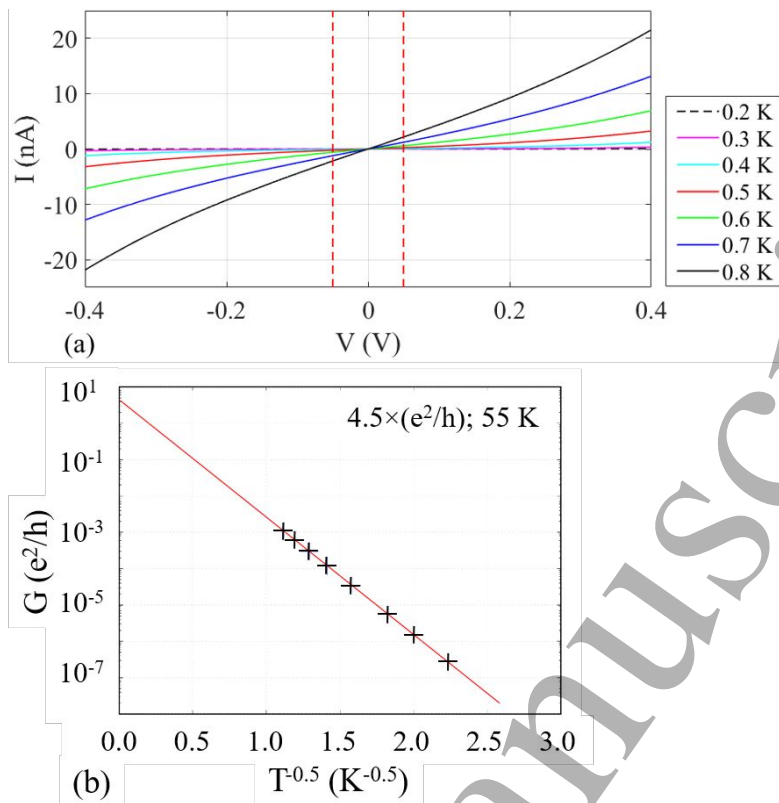
17

Figure 6. (a) The two-contact current voltage measurements on device Hall bar c(3) from wafer 2 down to 0.2 K. The red dotted lines (at ± 0.05 V) show the regions of applied voltages where a linear conductance can be determined, (b) The conductance (G) as a function $T^{-0.5}$ showing the Coulomb gap behaviour with temperature. For temperatures < 0.2 K the conductance is non-linear and this data is excluded from the fit. The actual fit to equation (3) (the red line) with q = 1/2 indicates an intercept of $4.5 \times (e^2/h)$ and a characteristic T_o of 55 K.
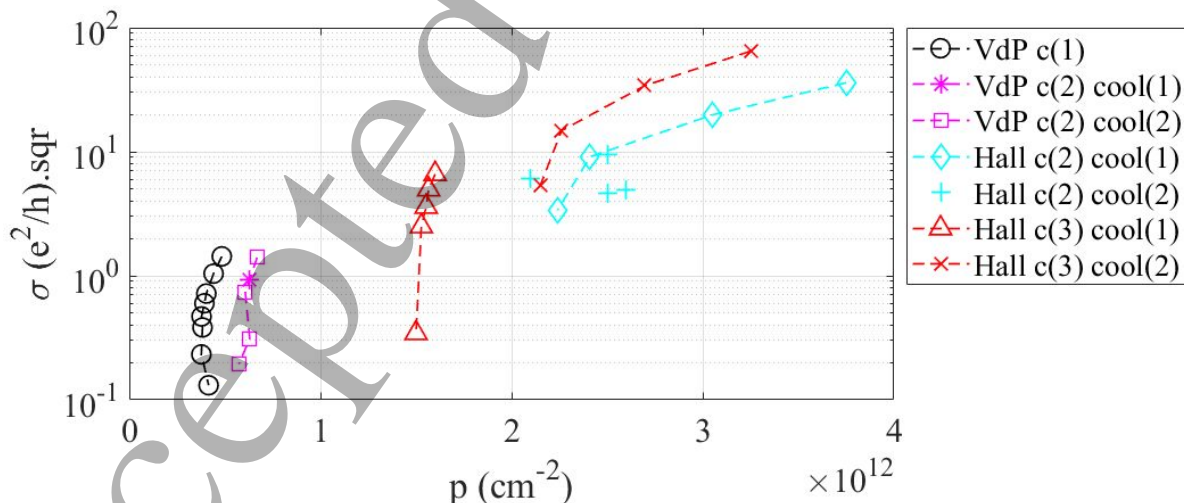

Figure 7. The conductivity as a function of carrier density in four different devices from wafer 2. The percolation behaviour of the conductivity at low temperature is discussed in section 3.

18